

**Repository of the Max Delbrück Center for Molecular Medicine (MDC)
in the Helmholtz Association**

<https://edoc.mdc-berlin.de/16920>

**Deletion of claudin-10 rescues claudin-16 deficient mice from
hypomagnesemia and hypercalciuria**

Breiderhoff T., Himmerkus N., Drewell H., Plain A., Günzel D., Mutig K., Willnow T.E.,
Müller D., Bleich M.

This is the final version of the accepted manuscript. The original article has been published in final edited form in:

Kidney International
2018 MAR; 93(3): 580-588
2017 NOV 10 (first published online: final publication)
doi: [10.1016/j.kint.2017.08.029](https://doi.org/10.1016/j.kint.2017.08.029)

Publisher: [Elsevier](#)



Copyright © 2017. This manuscript version is made available under the [Creative Commons Attribution-NonCommercial-NoDerivatives 4.0 International License](http://creativecommons.org/licenses/by-nc-nd/4.0/). To view a copy of this license, visit <http://creativecommons.org/licenses/by-nc-nd/4.0/> or send a letter to Creative Commons, PO Box 1866, Mountain View, CA 94042, USA.

Deletion of *claudin-10* rescues *claudin-16* deficient mice from hypomagnesemia and hypercalciuria

Tilman Breiderhoff^{1,5,*.§}, Nina Himmerkus^{2,*}, Hoorah Drewell³, Allein Plain², Dorothee Günzel⁴, Kerim Mutig³, Thomas E. Willnow⁵, Dominik Müller^{1.§}, Markus Bleich^{2.§}

¹Department of Pediatric Nephrology, Charité – Universitätsmedizin Berlin, 13353 Berlin, Germany

²Institute of Physiology, Christian-Albrechts-Universität zu Kiel, 24098 Kiel, Germany

³Institute of Vegetative Anatomy, Charité – Universitätsmedizin Berlin, 10117 Berlin, Germany

⁴Institute of Clinical Physiology, Charité – Universitätsmedizin Berlin, 12203 Berlin, Germany

⁵Max Delbrück Center for Molecular Medicine, 13125 Berlin, Germany

*T.B. and N.H. contributed equally to this work

§ Corresponding authors:

Tilman Breiderhoff

Department of Pediatric Nephrology,

Charité – Universitätsmedizin Berlin

Augustenburger Platz 1

13353 Berlin

Phone: +49 30 450516154

e-mail: tilman.breiderhoff@charite.de

Dominik Müller

Department of Pediatric Nephrology,

Charité – Universitätsmedizin Berlin

Augustenburger Platz 1

13353 Berlin

Phone: +49 30 450516015

e-mail: dominik.mueller@charite.de

Markus Bleich

Institute of Physiology

Christian-Albrechts-Universität zu Kiel

Olshausenstr. 40

24098 Kiel

Phone: +49 431 8802961

e-mail: m.bleich@physiologie.uni-kiel.de

Short Title: Deletion of *Cldn10* rescues symptoms of *Cldn16*^{-/-} mice

Keywords: paracellular pathway, tight junction, thick ascending limb, claudin, magnesium, calcium

Abstract

The tight junction proteins claudin-10 and claudin-16 are crucial for the paracellular reabsorption of cations along thick ascending limb of Henle's loop in the kidney. In humans, mutations of *CLDN16* cause familial hypomagnesemia with hypercalciuria and nephrocalcinosis, and mutations in *CLDN10* impair kidney function. Mice lacking claudin-16 display Mg^{2+} and Ca^{2+} wasting, while absence of claudin-10 results in hypermagnesemia and interstitial nephrocalcinosis. To study the functional interdependence of claudin-10 and claudin-16 we generated double-deficient mice. These mice had normal serum Mg^{2+} and urinary excretion of Ca^{2+} and Mg^{2+} , showed polyuria and Na^+ retention at the expense of increased renal K^+ excretion, but no nephrocalcinosis. Isolated thick ascending limb tubules of double mutants displayed a complete loss of paracellular cation selectivity and functionality. Mice lacking both claudin-10 and claudin-16 in the thick ascending limb recruited downstream compensatory mechanisms and showed hypertrophic distal convoluted tubules accompanied by changes in gene expression and phosphorylation of ion transporters in this segment, presumably triggered by the mild decrease in serum K^+ . Thus, we show that the severe individual phenotype in claudin-10 and claudin-16 knockout mice is corrected by the additional deletion of the other claudin, respectively.

Introduction

The tight junction (TJ) is a supramolecular structure forming strand-like connections between adjacent epithelial cells, thereby regulating paracellular permeability. The main constituent of the TJ strands are the claudins, which are tetraspanning membrane proteins that interact via their extracellular segments with claudins of the neighbouring cells. Claudins are either sealing the paracellular cleft or forming a channel thus conveying charge and size selectivity to the paracellular pathway ^{1,2}.

In humans, mutations in *CLDN16* cause the salt-wasting disorder familiar hypomagnesemia, hypercalciuria and nephrocalcinosis (FHHNC), characterized by renal loss of Ca^{2+} and Mg^{2+} , and by nephrocalcinosis. In most of the cases, FHHNC leads to end stage renal disease, ultimately requiring renal transplantation ³. Patients with mutations in *CLDN10* present with anhidrosis and mild kidney failure in one family or with a hypokalemic-alkalotic salt-losing tubulopathy in another family ⁴⁻⁶. Mice lacking claudin-16 display a pathology similar to that observed in FHHNC patients, i.e. hypomagnesemia and hypercalciuria ⁷. In sharp contrast, mice specifically lacking claudin-10 in the same part of the nephron display hypermagnesemia, hypocalciuria, nephrocalcinosis, and polyuria ⁸. Electrophysiological experiments in thick ascending limb (TAL) tubules lacking claudin-16 showed reduced paracellular Mg^{2+} and Ca^{2+} permeabilities ⁷. TAL tubules of *Cldn10*-deficient mice showed a reduced paracellular sodium permeability paralleled by an increased Mg^{2+} and Ca^{2+} permeability, and a higher expression of claudin-16 ⁸.

On the molecular basis, Claudin-10b forms paracellular cation channels, whereas permeability properties for mono- and divalent cations of claudin-16 alone or together with claudin-19 are still a matter of debate. The interaction of claudin-19 with claudin-16 is necessary for their

proper localization to the TJs and their co-expression has been reported to increase the paracellular permeability to cations in vitro ^{9,10}. In contrast, expression of claudin-14 reduces the paracellular permeability to cations and acts as negative modulator of paracellular transport of divalent cations in response to elevated levels of Ca^{2+} ^{11–13}. In the kidney claudin-10b is highly expressed in ISOM (inner stripe of the outer medulla), where paracellular transport of Na^+ predominates, while claudin-16 is restricted to the OSOM and cortex, where it colocalizes with claudin-19 ¹⁴. Claudin-10 and claudin-16 thereby do not colocalize in the same TJ strands and form a mosaic pattern, the permselectivity for Na^+ increasing with increasing percentage of Claudin-10 positive TJ strands. Based on our previous findings in mice lacking either claudin-16 or claudin-10 in the TAL and their expression profile, we hypothesized that claudin-10 and claudin-16 indeed contribute to different paracellular channels with different permeabilities to Na^+ , Ca^{2+} and Mg^{2+} ⁸. To test this hypothesis and to provide the basis for a better understanding of FHHNC, we generated mice lacking both, claudin-10 and claudin-16.

Results

We generated a mouse model lacking claudin-10 and claudin-16 by crossing claudin-16 deficient mice (C16 KO) ⁷ with mice lacking claudin-10 specifically in the kidney (C10 cKO) ⁸. Resulting double knockout mice (dKO) were born at Mendelian ratio, and were viable and fertile. We confirmed hypomagnesemia in C16 KO and hypermagnesemia in C10 cKO (Figure 1A). In contrast, in mice deficient for both claudins, serum Mg^{2+} concentration was in the range of control animals. Correspondingly, fractional excretion of Mg^{2+} (FE_{Mg}) was increased in C16 KO and decreased in C10 cKO, but normalized in dKO. While C16 KO mice showed a more than 3-fold increase in fractional excretion of Ca^{2+} (FE_{Ca}), dKO had urinary Ca^{2+} excretion levels comparable to controls (Figure 1B). Concomitantly, dKO showed no signs of nephrocalcinosis, a characteristic of hyperabsorption of divalent cations in C10 cKO (Figure 2).

The double deficient mice exhibited polyuria that they compensated by increased water intake (Table 1). Urinary pH was lower in all mouse models compared to control, ranging from a mild decrease in pH in C16 KO, to an intermediate acidity in the dKO, to a pronounced drop in urinary pH in C10 cKO mice. Na^+ , Cl^- and K^+ homeostasis was not affected in each of the single KO animal models. Interestingly, dKO animals, if compared to C16 KO, developed a mild but significant drop in plasma K^+ . Their increased FE_{K} was accompanied by a decrease in FE_{Na} indicating compensatory activity of the collecting duct to maintain salt balance.

Immunohistochemistry showed that claudin-16 and claudin-10 were differentially expressed along the cortico-medullary axis in the TAL (Figure 3). Claudin-10 immunoreactivity was found in cortex and medulla in basolateral structures and in TJs. Claudin-16 was restricted to TJs of cortex and outer stripe of outer medulla (OSOM) and absent in the inner stripe of outer medulla (ISOM). The mosaic distribution of claudin-10 and -16 was clearly visible in sections from control animals. In the ISOM only claudin-10 (Figure 3E,F), but in the cortex as well as in the OSOM, both claudins were expressed (Figure 3A,B). Whereas claudin-10 distribution remained unaltered in C16 KO (Figure 3D,H), claudin-16 expression extended to the ISOM in C10 cKO (Figure 3G). Both claudins were absent in dKO (data not shown).

Consequently, we investigated the electrophysiological properties of TAL tubules dissected either from the medulla (mTAL, ISOM) or from the cortical region (cTAL, cortex) of the kidney. mTAL from control animals showed an average transepithelial voltage (V_{te}) of 9 mV, an equivalent short circuit current (I'_{sc}) of $1300 \mu\text{A}/\text{cm}^2$ and a transepithelial resistance (R_{te}) of $8 \Omega\text{cm}^2$. Absence of claudin-10, -16, or both resulted in a significant increase in R_{te} with a concomitant decrease in I'_{sc} (Figure 4A). V_{te} was higher in C10 cKO mice. The effect of claudin

absence on resistance in mTAL was more prominent in tubules lacking claudin-10, the predominant claudin in the ISOM¹⁵.

In cTAL of C16 KO there was an increase in I'_{sc} while V_{te} and R_{te} tended to remain in the control range. In C10 cKO tubules R_{te} was not affected in cTAL but the tubules generated a highly significant increase in V_{te} reflecting a substantially increased transepithelial ion transport current I'_{sc} (Figure 4B). The absence of both claudins finally resulted in an increased R_{te} , a strongly reduced I'_{sc} , and V_{te} was normalized compared to controls (Figure 4B).

Changes in R_{te} were accompanied by altered paracellular selectivity properties of mTAL (Figure 5A). Whereas the permeability ratio P_{Na}/P_{Cl} in mTAL tubules of C16 KO was not different from control mice, mTAL of both C10 cKO and dKO kidneys displayed a strong loss in cation selectivity (decrease in P_{Na}/P_{Cl} ; Figure 5A). In accordance with the decreased P_{Na} in C10 cKO, the selectivity was significantly shifted to the divalent cations Ca^{2+} and Mg^{2+} (increase in P_{Ca}/P_{Na} and P_{Mg}/P_{Na} , respectively). In turn, when claudin-16 was additionally deleted in dKO, this shift to divalent cations was attenuated (Figure 5A).

In cTAL, similar to mTAL, the absence of claudin-16 did not affect P_{Na}/P_{Cl} , whereas claudin-10 deficiency resulted in a reduced P_{Na}/P_{Cl} (Figure 5B). cTAL in C10 cKO displayed a strong preference of the paracellular pathway for Ca^{2+} and Mg^{2+} . In contrast to the mTAL, the absence of claudin-16 in the cTAL caused a loss of Ca^{2+} and Mg^{2+} selectivity, as P_{Na}/P_{Cl} was unaltered but P_{Ca}/P_{Na} and P_{Mg}/P_{Na} was reduced. The deficiency for both claudins blunted the effects on Ca^{2+} and Mg^{2+} selectivity, resulting in a normalized P_{Ca}/P_{Na} and in a P_{Mg}/P_{Na} that was higher than in C16 KO but lower than in C10 cKO.

Using gene expression arrays, we identified genes differentially expressed in kidneys of the mouse models described in this study (Table 2). Claudin-19 expression was increased in the

dKO but unaltered in C16 KO and C10 cKO. While claudin-11 was expressed at significantly lower levels in both models lacking claudin-10, the expression of claudin-14 was comparable in all groups. Genes with a putative role in compensatory transcellular Ca^{2+} and Mg^{2+} handling in the downstream segment distal convoluted tubule (DCT) were also specially noted. *Slc8a1*, the gene encoding the basolateral Na^+ - Ca^{2+} -exchanger (NCX1) was expressed at higher levels in C16 KO and dKO mice while suppressed in the C10 cKO. Similarly, the expression of the Mg^{2+} channel TRPM6 was increased in the absence of claudin-16, but reduced in C10 cKO mice. In dKO animals, the expression of this Mg^{2+} channel was higher than in C16 KO animals and the expression of the Mg^{2+} transporter *Slc41a3* was higher than in C10 cKO. In addition, the expression of parvalbumin and CNNM2, both involved in DCT Mg^{2+} handling, was increased in dKO in comparison to control and C10 cKO mice. The CaSR, a key regulator of divalent cation metabolism was expressed at similar levels in mice of different genotype.

As these findings were indicative for compensatory mechanisms in dKO especially in the DCT we investigated this nephron segment in more detail (Figure 6). Immunohistochemical staining of the sodium chloride cotransporter NCC (*Slc12a3*) to mark DCTs in kidney slices revealed a strong hypertrophy of this segment in dKO (Figure 6A). The fractional volume of this tubular segment was increased by 90% in comparison to control animals and to C16 KO (Figure 6A,B). NCC is the key salt transporting protein in DCT and its activity is mainly controlled by its phosphorylation state. Total protein amount as well as phosphorylation state were increased in dKO corroborating a compensatory hyperfunction of this segment (Figure 6C,D).

Compensatory changes in sodium transport protein expression in other nephron segments were also assessed by western blot analysis (see supplemental Figure). In TAL the expression of NKCC2 remained unchanged, but the phosphorylation of NKCC2 is increased in dKOs when compared to controls. However, this does not translate in restoring of effective NaCl transport as shown in Figure 4B. In contrast, collecting duct and proximal tubule did not indicate

comparable compensatory changes and the expression of NHE3 (proximal tubule) and γ -ENaC (connecting tubule and collecting duct) were without substantial changes between genotypes.

Discussion

The loss of Ca^{2+} and Mg^{2+} in C16 KO and in FHHNC patients, respectively, has been explained primarily by the defect in the major paracellular pathway for these divalent cations in the TAL ⁷. Neither the proximal tubule nor the DCT were able to compensate for this defect in C16 KO. However, although the paracellular pathway was virtually absent in the TAL of dKO, they had normal urinary and serum levels of Ca^{2+} and Mg^{2+} . We hypothesize that this is based on the differences in salt and water handling in dKO in comparison to control animals and the single knock-out models.

The TAL is the motor of the concentration ability of the kidney by moving NaCl from the lumen into the interstitium of the outer medulla. This active transport by the TAL generates a lumen positive potential which is used secondarily to reabsorb cations. In the medulla, 50% of Na^+ reabsorption is driven paracellularly by this potential, while in the cortical parts, it drives Ca^{2+} , Mg^{2+} and Na^+ ¹⁶. Accordingly, in the medulla claudin-10 but not claudin-16 is present in the TJ (Figure 3), whereas, in cortical parts of the TAL claudin-10 and claudin-16 positive TJ are found in parallel in a mosaic pattern ¹⁴ (Figure 3 and 7).

Considering these differences in transport and claudin expression along the cortico-medullary axis isolated perfused mTAL and cTAL have been investigated separately. A qualitative estimate of paracellular ion permeation can be obtained considering R_{te} , the selectivity between cations and anions ($P_{\text{Na}}/P_{\text{Cl}}$) and the ratio for the respective cation permeabilities (Figure 4 and Figure 5). The pathophysiology of the paracellular transport in the mTAL is dominated by claudin-10 ¹⁵ (Figure 7). Whereas there was high paracellular cation selectivity ($P_{\text{Na}}/P_{\text{Cl}}$) in

control and claudin-16 deficient mTAL, the cation selectivity of the paracellular pathway was abolished in claudin-10 deficient mTAL. As R_{te} was not increased in C10 cKO, the increase in Ca^{2+} and Mg^{2+} transport is caused by the increase in the permeability for Ca^{2+} and Mg^{2+} , compensating the decrease in Na^+ permeability by deletion of claudin-10. The morphological correlate for this observation is expansion of claudin-16 into the mTAL. The second factor for increased transport of Ca^{2+} and Mg^{2+} in mTAL is V_{te} . Obviously, the absence of claudin-10 generates an increased driving force for hyperabsorption of divalent cations in C10 cKO resulting in medullary nephrocalcinosis. In dKO, this shift to divalent cation reabsorption was abolished by the additional loss of claudin-16 (Figure 7) and the mTAL lost tight junction selectivity ($P_{Na}/P_{Cl} \approx 1$) and permeability (R_{te} increased). Although the driving force V_{te} was still present in dKO tubules there was no longer interstitial calcification, underscoring the importance of claudin-16 expansion to mTAL for the C10 cKO phenotype. The reduction of Na^+ transport (I'_{sc}) in mTAL of dKO was most likely due the high paracellular resistance. As a result, the luminal fluid leaving the mTAL was less diluted and the interstitium less concentrated. This limited TAL function with limited salt and water conservation in dKO lead to polyuria as the renal concentration mechanism was impeded and to a salt load downstream of the TAL.

Claudin-16 was expressed at higher levels in cTAL, but the absence of claudin 16 resulted in normal R_{te} and V_{te} , in this segment, and the selectivity for cations was not different from controls, reflecting an intact paracellular permeation pathway for Na^+ (Figure 7). However, C16 KO led to a strong reduction in the contribution of Ca^{2+} to cation permeability (P_{Ca}/P_{Na}) and hence to the loss of Ca^{2+} via TAL. Another parameter which contributes to paracellular Ca^{2+} and Mg^{2+} transport especially in cTAL is the diffusion voltage of the TAL. It is also lumen positive and depends on a gradient for NaCl from the interstitium to the lumen (dilute luminal fluid) and on the cation selectivity of the paracellular pathway. Both prerequisites are impeded in dKO TAL as mentioned above. Since claudin-16 is missing in addition, there is no relevant route for

paracellular Ca^{2+} transport, which is in contrast to the situation in C10 cKO where claudin-16 even extended to the medulla.

Cation channel properties of claudin-16 are still a matter of debate as there is a lack of a suitable cell line that mimics paracellular TAL properties¹⁷. Considering the TJ mosaic in the cTAL we could show that an increasing percentage of claudin-16 positive TJ correlates with increasing $P_{\text{Mg}}/P_{\text{Na}}$ ¹⁴. In the present study, comparison of TAL permeabilities from C10 cKO and dKO animals allow to estimate the effects of claudin-16 in the absence of any further channel-forming and thus potentially interfering claudins. In the cortex, deletion of claudin-16 in the absence of claudin-10 causes a substantial reduction in $P_{\text{Mg}}/P_{\text{Na}}$ and $P_{\text{Ca}}/P_{\text{Na}}$ together with an increase in R_{te} . This indicates that Mg^{2+} as well as Ca^{2+} permeabilities are dramatically reduced. In the medulla, the reduction of $P_{\text{Mg}}/P_{\text{Na}}$ and $P_{\text{Ca}}/P_{\text{Na}}$ is less pronounced and R_{te} remains constant. This is in line with a low but effective medullary claudin-16 expression in C10 cKO. Thus, the present results affirm the fundamental contribution of claudin-16 towards divalent cation permeability in the TAL.

The absence of one claudin often results in the changed expression of other claudins. In kidneys of the dKO claudin-11 was expressed at lower levels whereas claudin-19 was expressed at higher levels. Claudin-11 and claudin-19 are considered to possess sealing properties^{9,18,19}. However, claudin-11 KO mice as well as claudin-11/claudin-14 double deficient animals do not show significant changes in renal Ca^{2+} or Mg^{2+} handling under standard dietary conditions²⁰. Claudin-19 is interacting with claudin-16 and mutations in *CLDN19* lead to FHHNC. Claudin-19 deficiency in mice leads to a phenotype reminiscent of claudin-16 deficiency^{9,10,21}. It is still debated if claudin-19 forms a paracellular pore itself, but changes in the expression of claudin-19 alone, or together with other moderately expressed TAL claudins (claudin-3, claudin-11) might alter tight junction composition and Ca^{2+} and Mg^{2+} permeability resulting in the residual preference to divalent cations in the dKO TAL (Figure 5).

Besides these TAL findings this study also gives some interesting insights into renal regulation and compensation abilities. Regarding Ca^{2+} and Mg^{2+} metabolism, the dKO can cope better than C10 cKO and especially than C16 KO, although there is no evidence for improvement of divalent cation reabsorption in the cTAL itself. Compensatory response of the DCT downstream to the TAL was therefore the second focus of the present study (Figure 7). To summarize the expression studies on mRNA level C16 KO increased and C10 cKO decreased DCT transport of NaCl (e.g. NCC) and Ca^{2+} and Mg^{2+} (e.g. NCX1, TRPM6, Table 2). dKO, however, showed a massive compensatory response with a clearly visible increase in fractional DCT volume indicating a sustained physiologic perturbation which promoted structural remodeling of the DCT epithelium (Figure 6A). Thereby, dKO mice with their primary defect in the paracellular pathway did not show very severe salt wasting. In C10 cKO claudin-10 as main cation selective claudin is missing too, however, claudin-16 likely allows partially Na^+ absorption, although Na^+ permeability of claudin-16 has been discussed controversially in cell culture expression systems^{9,22}. Whereas C16 KO and C10 cKO only showed steady-state disturbance in their serum Mg^{2+} concentrations, dKO showed a slight reduction in serum K^+ , a decrease in FE_{Na^+} and increase in FE_{K^+} , revealing sodium conservation on the expense of K^+ loss downstream the TAL. DCT, the connecting tubule and the collecting duct are on the one hand stimulated by systemic hormones like aldosterone and on the other hand challenged by increased luminal NaCl delivery. DCT has two principal mechanisms to increase its transport rate. Dietary NaCl restriction leads mainly to increase of transport capacity by expression and phosphorylation, whereas high rates of luminal ion delivery strongly induce an increase in fractional volume of DCT cells as shown in rats under chronic therapy with loop diuretics²³. Both mechanisms are likely recruited in dKO kidneys. NCC phosphorylation is a strong indicator of NCC activity and we show a consistent massive increase in pNCC in dKO in comparison to control animals. Lower serum K^+ concentrations, only present in dKO, and stimulation of the WNK pathway

might be causative for this ^{24,25}. The massive hypertrophy and hyperplasia of DCT cells which multiplies the transport capacity strongly supports the hypothesis that the TAL of dKO is virtually non-functional and delivering an increased ion load to the DCT. Consequently, the electrolyte homeostasis in dKO animals might be comparable to mice chronically treated with furosemide, in which the inhibition of TAL transport also does not affect urinary excretion of Ca^{2+} or serum levels of Mg^{2+} ²⁶. We found no conclusive evidence for a compensatory contribution of CD on expression level.

Increase in proximal tubular salt and water transport (beyond increase in total NHE3 protein expression) might serve as additional compensatory back-up for Ca^{2+} reabsorption. In *Trpv5* KO mice without functional transcellular Ca^{2+} reabsorption the inhibition of DCT NaCl transport is still effectively increasing renal Ca^{2+} conservation secondary to diuretic therapy induced volume loss ^{27,28,29}.

Renal compensation response to TAL transport defects obviously depends on the transport property which is specifically affected (trans- or paracellular), on the localization of the defect (mTAL, cTAL or beyond TAL) as well as on its severity (transcellular NaCl transport primarily or secondarily affected).

Taken together (Figure 7), we show that the elimination of claudin-10 and claudin-16 severely impairs the cation-selective paracellular pathway in the TAL and its functionality in NaCl transport. However, the double-deficiency rescues deranged homeostasis of divalent cations in the single knockout animals, likely by affecting salt and water balance and thereby recruiting additional compensatory mechanisms. This observation might inspire the development of new therapeutic concepts for the treatment of FHHNC.

Material and Methods

Generation of *Cldn10/Cldn16*-deficient mice. Mice homozygous for the floxed *Cldn10* allele and ksp-Cre positive (*Cldn10^{fl/fl} cre⁺*)⁸ were bred with mice homozygous for the deleted *Cldn16* allele (*Cldn16^{-/-}*)⁷. Resulting double heterozygous were bred with each other to generate *Cldn16^{-/-} Cldn10^{fl/fl} cre⁺* animals. We did not observe differences between *Cldn16^{+/-}* and *Cldn16^{+/+}* animals and subsequently bred *Cldn16^{-/-} Cldn10^{fl/fl} cre⁻* to *Cldn16^{+/-} Cldn10^{fl/fl} cre⁺* for the efficient generation of double mutant animals. The analysed animals were littermates with the following genotype: control mice (con) - *Cldn16^{+/-}, Cldn10^{fl/fl}, ksp-cre⁻*; claudin-16 deficient mice (C16 KO) - *Cldn16^{-/-}, Cldn10^{fl/fl}, ksp-cre⁻*; claudin-10 deficient mice (C10 cKO) - *Cldn16^{+/-}, Cldn10^{fl/fl}, ksp-cre⁺*, claudin-10/16 deficient mice (dKO) - *Cldn16^{-/-}, Cldn10^{fl/fl}, ksp-cre⁺*. The genetic background of the mice is C57Bl/6N (>97%).

Antibodies Primary antibodies were rabbit-anti-claudin-10, mouse-anti-occludin (ThermoFisher Scientific), rabbit-anti-claudin-16 (provided by J Hou)¹¹, rabbit-anti-NCC and rabbit-anti-pNCC (provided by DH Ellison) rabbit-anti-NKCC2³⁰, guinea-pig-anti-pNKCC2³¹, rabbit-anti-eNaC (γ -subunit) and rabbit-anti-NHE3 (biotrend), and mouse-anti-tubulin (abcam). Secondary antibodies were coupled to Alexa Fluor 488 or 555 or horseradish peroxidase (ThermoFisher Scientific).

Histology and immunohistochemistry Mice were perfused with 4% (w/v) PFA in PBS and isolated tissues were fixed in 4% PFA in PBS overnight at 4°C. Tissues were dehydrated with alcohol and xylene, and embedded in paraffin. 10 μ m paraffin sections were rehydrated with xylene and alcohol.

For von Kossa staining, sections were incubated for 20 min in 1% silver nitrate under UV exposure. After rinsing and incubation in 5% NaS₂O₃, tissues were counterstained with eosin, dehydrated in xylene and mounted using DPX mountant (Sigma).

Immunohistochemistry was performed after antigen retrieval with sodium citrate pH 6.0. Sections were incubated in PBS supplemented with 0.3 % Triton X-100 and 5 % milk powder. After incubation with the primary antibody overnight, sections were incubated for 1 h with the respective secondary antibodies, and mounted with Fluorescence Mounting Medium (DAKO). Confocal images were acquired using a Leica TCS SPE microscope.

For morphometric analysis the fractional volume of DCT segments among strains was evaluated by light microscopy according to previously described techniques²³. Briefly, 5 µm-thick paraffin sections were stained for NCC to identify DCT. Cortical areas extending between the renal capsule and the outer medullary boundary were assessed. Sections were photographed and printed at a final magnification of ×100. At least three prints per animal were evaluated.

Urine and blood parameters. Urine samples were collected from mice placed in metabolic cages for 17 h. Blood sampling was performed by retro-orbital puncture. Ion concentrations in urine and serum were measured using a standard clinical analyzer or colorimetric detection (Magnesium Quantichrom assay, Gentaur). Creatinine analysis was carried out using a Hitachi Analyzer. Whereas urinary creatinine analysis produced reliable values, all plasma creatinine values were below detection limit (0.02 mM) indicating no evident renal failure in any of the investigated groups of animals. Additionally, we measured serum creatinine in mice older than three months and found no differences (con: 0.13 ± 0.001 µM, C16 KO: 0.014 ± 0.004 µM, C10 cKO: 0.11 ± 0.001 µM, dKO: 0.012 ± 0.001 µM). For calculation of fractional excretion plasma creatinine was assumed to be constant with a value of 0.015 mM for all animals of all groups

using the equation: $[X]_{urine} \cdot \text{const.} \cdot [\text{crea}]_{plasma} / ([X]_{plasma} \cdot [\text{crea}]_{urine})$. All experimental procedures in animals were conducted according to the guidelines for proper conduct of animal experiments and approved by the institutional animal care and use committee in Kiel and by the LaGeSo in Berlin.

Renal tubule perfusion. The methods for perfusion and transepithelial measurements in freshly isolated mouse TAL segments were performed as described previously³². cTAL and mTAL were isolated mechanically from thin coronary sections at 4°C within 2 h after mouse death. Tubules were transferred into the bath on a heated microscope stage held and perfused by a concentric glass pipette system with a rate of 10-20 nl/min. A double-barreled perfusion pipette with an outer diameter of 10-12 μm was used. Barrel 1 served for perfusion, fluid exchange, and voltage measurement. Barrel 2 was used for constant, pulsed current injection (13 nA). R_{te} was calculated by cable equations³². I'_{sc} was calculated from R_{te} and V_{te} according to Ohms law. Continuous bath perfusion at 3-5 ml/min was obtained by gravity. Composition of the solutions used is listed in Table S1. Transcellular transport was measured under symmetrical luminal and basolateral perfusion with control solution (Ctrl) and after luminal application of 50 μM furosemide in Ctrl. In the continuous presence of luminal furosemide, basolateral fluids were replaced by modified solutions. For measurements of dilution potentials and the calculation of P_{Na}/P_{Cl} , NaCl was diluted iso-osmotically at the basolateral side (solution 30 mM NaCl). Bi-ionic diffusion potentials were then measured after basolateral replacement of Ctrl by solutions containing 72.5 mM MgCl_2 or 72.5 mM CaCl_2 , respectively, and no Na^+ (Table S1). Permeability ratios were calculated according to Günzel et al.³³.

Gene expression array. Mice were killed by cervical dislocation. Kidneys were isolated and immediately homogenized in TriZOL (Thermo Fisher Scientific). After chloroform extraction,

RNA was isolated from the aqueous phase using RNeasy columns (Qiagen). cRNA was produced using Illumina TotalPrep RNA Amplification Kit (Ambion) and hybridized to MouseWG-6 v2.0 Expression BeadChip Kit (Illumina). Data were normalized and analyzed using the GenomeStudio (Illumina).

Western Blot. Western Blot analysis of kidney membrane preparations were performed as previously described ⁸. In brief, kidneys were homogenized with an Ultra-Turrax in homogenization buffer [140 mM NaCl, 20 mM Tris (pH 7.5), 1 mM EDTA] with protease inhibitors (Complete; Roche) and phosphatase inhibitors (PhosSTOP, Roche) and cleared by centrifugation at 1,000×g for 10 min. Membranes were pelleted at 100,000×g for 30 min and then resuspended in homogenization buffer supplemented with protease/phosphatase inhibitors and 2% (wt/vol) SDS. Equal amounts (10 µg) of protein were separated by SDS/PAGE and blotted onto PVDF membrane. After blocking, membranes were incubated with indicated antisera, washed, incubated with HRP-coupled secondary antisera and washed again. HRP was visualized with a Fuji LAS-1000 luminescent image analyzer. Densitometric quantifications were performed using ImageJ.

Statistics.

Values are expressed as means ± SEM. Statistical significance was calculated with one-way ANOVA with Holm-Bonferroni post hoc testing for multiple comparisons. A *P* value of <0.05 was considered significant.

Acknowledgements

This work is supported by the Berlin Institute of Health Grant CRG2bTP4 to DM and by the DFG Grant GU 447/14-1 to DG. We thank J. Hou (Washington University in St. Louis) and D.H.

Ellison (Oregon Health and Care University) for sharing reagents, and M. Schmeisser, K. Kampf, T. Stegmann, R. Lingg, and K. Sommer for excellent technical assistance.

Disclosure statement

The authors have no competing financial interests.

References

1. Günzel D, Yu ASL. Claudins and the modulation of tight junction permeability. *Physiol. Rev.* 2013; **93**: 525–569.
2. Furuse M, Sasaki H, Tsukita S. Manner of interaction of heterogeneous claudin species within and between tight junction strands. *J. Cell Biol.* 1999; **147**: 891–903.
3. Weber S, Schneider L, Peters M *et al.* Novel paracellin-1 mutations in 25 families with familial hypomagnesemia with hypercalciuria and nephrocalcinosis. *J. Am. Soc. Nephrol. JASN* 2001; **12**: 1872–1881.
4. Bongers EMHF, Shelton LM, Milatz S *et al.* A Novel Hypokalemic-Alkalotic Salt-Losing Tubulopathy in Patients with CLDN10 Mutations. *J. Am. Soc. Nephrol. JASN* 2017, <https://doi.org/10.1681/ASN.2016080881>.
5. Klar J, Piontek J, Milatz S *et al.* Altered paracellular cation permeability due to a rare CLDN10B variant causes anhidrosis and kidney damage. *PLoS Genet.* 2017; **13**: e1006897.
6. Hadj-Rabia S, Brideau G, Al-Sarraj Y *et al.* Multiplex epithelium dysfunction due to CLDN10 mutation: the HELIX syndrome. *Genet. Med.* 2017, <https://doi.org/10.1038/gim.2017.71>.
7. Will C, Breiderhoff T, Thumfart J *et al.* Targeted deletion of murine Cldn16 identifies extra- and intrarenal compensatory mechanisms of Ca²⁺ and Mg²⁺ wasting. *Am. J. Physiol. Renal Physiol.* 2010; **298**: F1152-1161.
8. Breiderhoff T, Himmerkus N, Stuiver M *et al.* Deletion of claudin-10 (Cldn10) in the thick ascending limb impairs paracellular sodium permeability and leads to hypermagnesemia and nephrocalcinosis. *Proc. Natl. Acad. Sci. U. S. A.* 2012; **109**: 14241–14246.
9. Hou J, Renigunta A, Konrad M *et al.* Claudin-16 and claudin-19 interact and form a cation-selective tight junction complex. *J. Clin. Invest.* 2008; **118**: 619–628.
10. Hou J, Renigunta A, Gomes AS *et al.* Claudin-16 and claudin-19 interaction is required for their assembly into tight junctions and for renal reabsorption of magnesium. *Proc. Natl. Acad. Sci. U. S. A.* 2009; **106**: 15350–15355.
11. Gong Y, Renigunta V, Himmerkus N *et al.* Claudin-14 regulates renal Ca²⁺ transport in response to CaSR signalling via a novel microRNA pathway. *EMBO J.* 2012; **31**: 1999–2012.
12. Gong Y, Hou J. Claudin-14 Underlies Ca⁺⁺-Sensing Receptor-Mediated Ca⁺⁺ Metabolism via NFAT-microRNA-Based Mechanisms. *J. Am. Soc. Nephrol. JASN* 2013.
13. Gong Y, Himmerkus N, Plain A *et al.* Epigenetic regulation of microRNAs controlling CLDN14 expression as a mechanism for renal calcium handling. *J. Am. Soc. Nephrol. JASN* 2015; **26**: 663–676.

14. Milatz S, Himmerkus N, Wulfmeyer VC *et al.* Mosaic expression of claudins in thick ascending limbs of Henle results in spatial separation of paracellular Na⁺ and Mg²⁺ transport. *Proc. Natl. Acad. Sci. U. S. A.* 2017; **114**: E219–E227.
15. Plain A, Wulfmeyer VC, Milatz S *et al.* Corticomedullary difference in the effects of dietary Ca²⁺ on tight junction properties in thick ascending limbs of Henle's loop. *Pflüg. Arch. Eur. J. Physiol.* 2016; **468**: 293–303.
16. Himmerkus N, Plain A, Marques RD *et al.* AVP dynamically increases paracellular Na(+) permeability and transcellular NaCl transport in the medullary thick ascending limb of Henle's loop. *Pflugers Arch.* 2017; **469**: 149–158.
17. Günzel D, Yu ASL. Function and regulation of claudins in the thick ascending limb of Henle. *Pflüg. Arch. Eur. J. Physiol.* 2009; **458**: 77–88.
18. Van Itallie CM, Fanning AS, Anderson JM. Reversal of charge selectivity in cation or anion-selective epithelial lines by expression of different claudins. *Am. J. Physiol. Renal Physiol.* 2003; **285**: F1078-1084.
19. Angelow S, El-Husseini R, Kanzawa SA *et al.* Renal localization and function of the tight junction protein, claudin-19. *Am. J. Physiol. Renal Physiol.* 2007; **293**: F166-177.
20. Elkouby-Naor L, Abassi Z, Lagziel A *et al.* Double gene deletion reveals lack of cooperation between claudin 11 and claudin 14 tight junction proteins. *Cell Tissue Res.* 2008; **333**: 427–438.
21. Konrad M, Schaller A, Seelow D *et al.* Mutations in the tight-junction gene claudin 19 (CLDN19) are associated with renal magnesium wasting, renal failure, and severe ocular involvement. *Am. J. Hum. Genet.* 2006; **79**: 949–957.
22. Kausalya PJ, Amasheh S, Günzel D *et al.* Disease-associated mutations affect intracellular traffic and paracellular Mg²⁺ transport function of Claudin-16. *J. Clin. Invest.* 2006; **116**: 878–891.
23. Ellison DH, Velázquez H, Wright FS. Adaptation of the distal convoluted tubule of the rat. Structural and functional effects of dietary salt intake and chronic diuretic infusion. *J. Clin. Invest.* 1989; **83**: 113–126.
24. Castañeda-Bueno M, Cervantes-Perez LG, Rojas-Vega L *et al.* Modulation of NCC activity by low and high K(+) intake: insights into the signaling pathways involved. *Am. J. Physiol. Renal Physiol.* 2014; **306**: F1507-1519.
25. Terker AS, Zhang C, McCormick JA *et al.* Potassium modulates electrolyte balance and blood pressure through effects on distal cell voltage and chloride. *Cell Metab.* 2015; **21**: 39–50.
26. van Angelen AA, Kemp AW van der, Hoenderop JG *et al.* Increased expression of renal TRPM6 compensates for Mg²⁺ wasting during furosemide treatment. *Clin. Kidney J.* 2012; **5**: 535–544.

27. Nijenhuis T, Vallon V, van der Kemp AWCM *et al.* Enhanced passive Ca²⁺ reabsorption and reduced Mg²⁺ channel abundance explains thiazide-induced hypocalciuria and hypomagnesemia. *J. Clin. Invest.* 2005; **115**: 1651–1658.
28. Reilly RF, Huang C-L. The mechanism of hypocalciuria with NaCl cotransporter inhibition. *Nat. Rev. Nephrol.* 2011; **7**: 669–674.
29. Mensenkamp AR, Hoenderop JGJ, Bindels RJM. Recent advances in renal tubular calcium reabsorption. *Curr. Opin. Nephrol. Hypertens.* 2006; **15**: 524–529.
30. Reiche J, Theilig F, Rafiqi FH *et al.* SORLA/SORL1 functionally interacts with SPAK to control renal activation of Na(+)-K(+)-Cl(-) cotransporter 2. *Mol. Cell. Biol.* 2010; **30**: 3027–3037.
31. Schmitt R, Klusmann E, Kahl T *et al.* Renal expression of sodium transporters and aquaporin-2 in hypothyroid rats. *Am. J. Physiol. Renal Physiol.* 2003; **284**: F1097-1104.
32. Greger R. Cation selectivity of the isolated perfused cortical thick ascending limb of Henle's loop of rabbit kidney. *Pflüg. Arch. Eur. J. Physiol.* 1981; **390**: 30–37.
33. Günzel D, Stuver M, Kausalya PJ *et al.* Claudin-10 exists in six alternatively spliced isoforms that exhibit distinct localization and function. *J. Cell Sci.* 2009; **122**: 1507–1517.

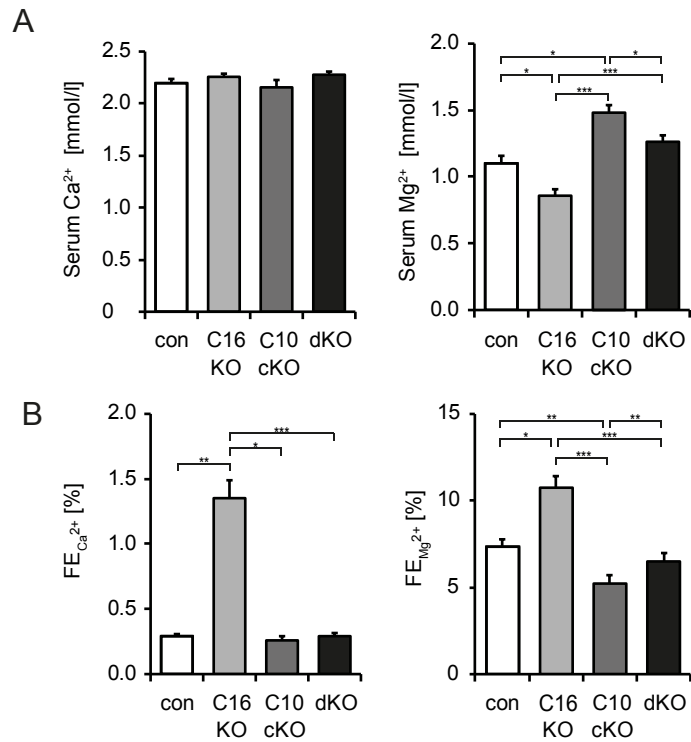


Figure 1 Homeostasis of Ca²⁺ and Mg²⁺

Summarized data are shown for serum Ca²⁺ and Mg²⁺ concentrations (A) and fractional excretions (FE) of these divalent ions (B). In contrast to C16 KO (hypomagnesemia) and C10 cKO (hypermagnesemia), dKO show normalized Mg²⁺ concentrations. The hypercalciuria and hypermagnesuria of C16 KO (shown as increased FE_{Ca²⁺} and FE_{Mg²⁺}) is normalized in dKO. Data are shown as mean ± SEM, n = 5-11. * p<0.05, ** p<0.01, *** p<0.001 in one-way ANOVA with Holm-Bonferroni post-hoc test.

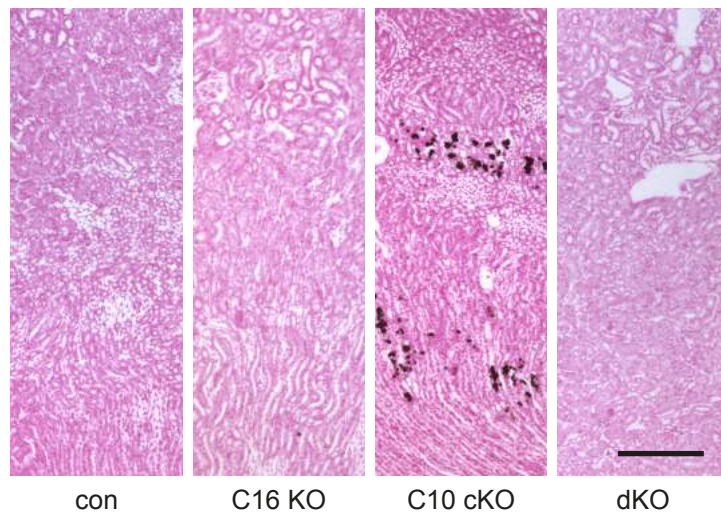


Figure 2 Absence of nephrocalcinosis in kidneys of C10C16dKOs

Strong Von Kossa staining of deposits is only found in kidney sections from C10 cKO mice but neither in C16 KO nor in C10C16 dKO mice. Sections were counterstained with eosin. Scale bar 1 mm

	control	C16 KO	<i>P</i> C16 vs. con	C10 cKO	<i>P</i> C10 vs. con	<i>P</i> C10 vs. C16	dKO	<i>P</i> dKO vs. con	<i>P</i> dKO vs. C16 KO	<i>P</i> dKO vs. C10 cKO
volume [ml/24h]	2,2 ± 0,2	2,9 ± 0,2		5,8 ± 0,6	***	***	6,1 ± 0,3	***	***	
osmolality [mosm/kg]	928 ± 43	898 ± 39		503 ± 37	***	***	463 ± 8	***	***	
pH	6,12 ± 0,05	5,93 ± 0,04	*	5,30 ± 0,05	***	***	5,50 ± 0,04	***	***	**
FE _{Na+} [%]*	0,37 ± 0,01	0,42 ± 0,02		0,34 ± 0,01			0,32 ± 0,01	**	***	
FE _{K+} [%]*	15,83 ± 0,37	16,32 ± 0,44		16,95 ± 0,51			22,17 ± 0,66	***	***	**
FE _{Cl-} [%]*	0,74 ± 0,03	0,74 ± 0,03		0,55 ± 0,03	**	**	0,66 ± 0,02			
FE _{Ca2+} [%]*	0,29 ± 0,02	1,35 ± 0,14	***	0,26 ± 0,03		***	0,29 ± 0,03		***	
FE _{Mg2+} [%]*	7,32 ± 0,42	10,74 ± 0,66	**	5,20 ± 0,52	*	***	6,51 ± 0,46		***	
Na ⁺ [mM]	153,5 ± 1,1	150,2 ± 0,9		154,0 ± 2,0			153,7 ± 0,8			
K ⁺ [mM]	5,2 ± 0,2	5,6 ± 0,2		5,2 ± 0,1			4,7 ± 0,2		**	
Cl ⁻ [mM]	99,8 ± 1,4	99,2 ± 1,5		101,1 ± 3,3			96,7 ± 0,9			
Ca ²⁺ [mM]	2,2 ± 0,0	2,3 ± 0,0		2,1 ± 0,1			2,3 ± 0,0			
Mg ²⁺ [mM]	1,1 ± 0,1	0,9 ± 0,0	**	1,5 ± 0,1	***	***	1,3 ± 0,0		***	**
	n ≥ 11	n ≥ 12		n ≥ 5			n ≥ 6			

Table 1 Serum and urine parameters in control- and KO mice

Urine parameters and serum electrolyte concentrations from metabolic cage experiments. Data are shown as mean ± SEM. * p<0.05, ** p<0.01, *** p<0.001 in one-way ANOVA with Holm-Bonferroni post-hoc test

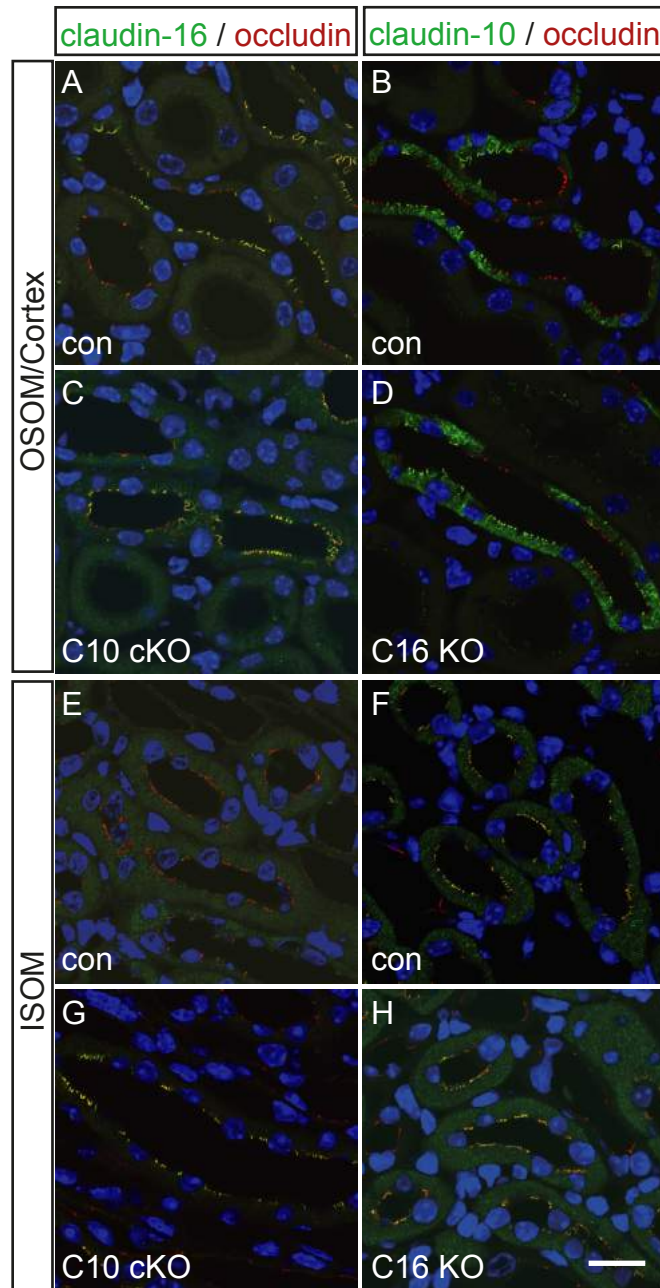
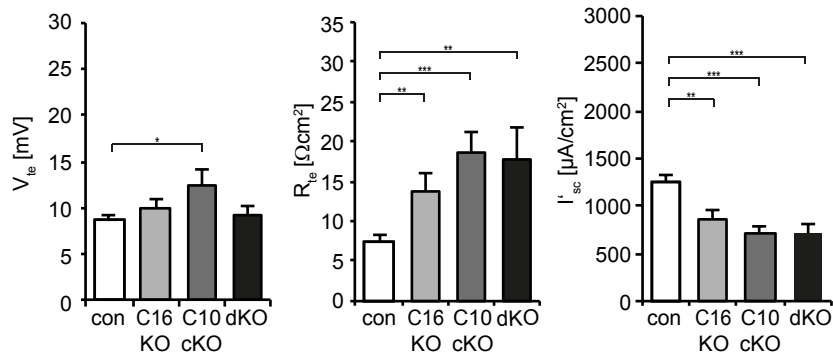


Figure 3 Immunolocalization of claudin-10 and claudin-16 along the cortico-medullary axis.

(A) In controls, claudin-16 (A) and claudin-10 (B) are expressed in the cortex and the outer stripe of outer medulla (OSOM) but only claudin-10 in the inner stripe of outer medulla (ISOM) (F). While tubules from C16 KO show an un-altered claudin-10 distribution (D,H), expression of claudin-16 expands to ISOM tubules from C10 cKO (G) while it was absent in ISOM from controls (E). In contrast, C10 cKO did not affect the expression pattern of claudin-16 in OSOM/Cortex (C). Scale bar 25 μ m

A medullary



B cortical

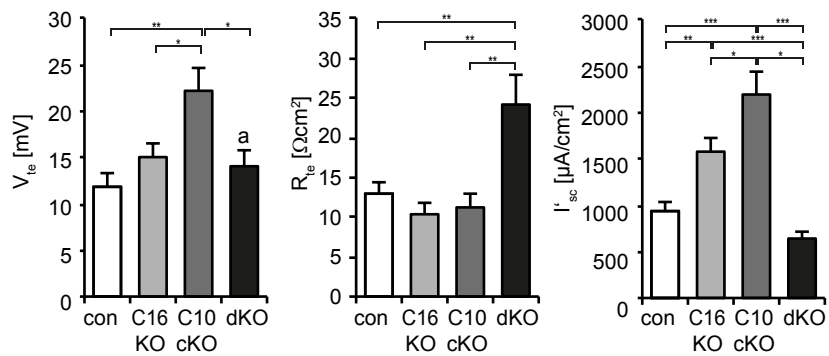


Figure 4 Electrophysiological properties of isolated perfused mTAL and cTAL

Summarized electrophysiological properties of mTAL (A) and cTAL (B) tubules: (A) In mTAL, V_{te} is elevated in C10 cKO vs. control. All KO models exhibit a higher resistance and a decreased transport current. (B) In cTAL, V_{te} is increased in C10 cKO and R_{te} shows a massive increase only in dKO. Transcellular transport current is increased in both single KO models but normalized in dKO. Data are shown as mean \pm SEM. $n=9-15$. * $p<0.05$, ** $p<0.01$, *** $p<0.001$ in one-way ANOVA with Holm-Bonferroni post-hoc test.

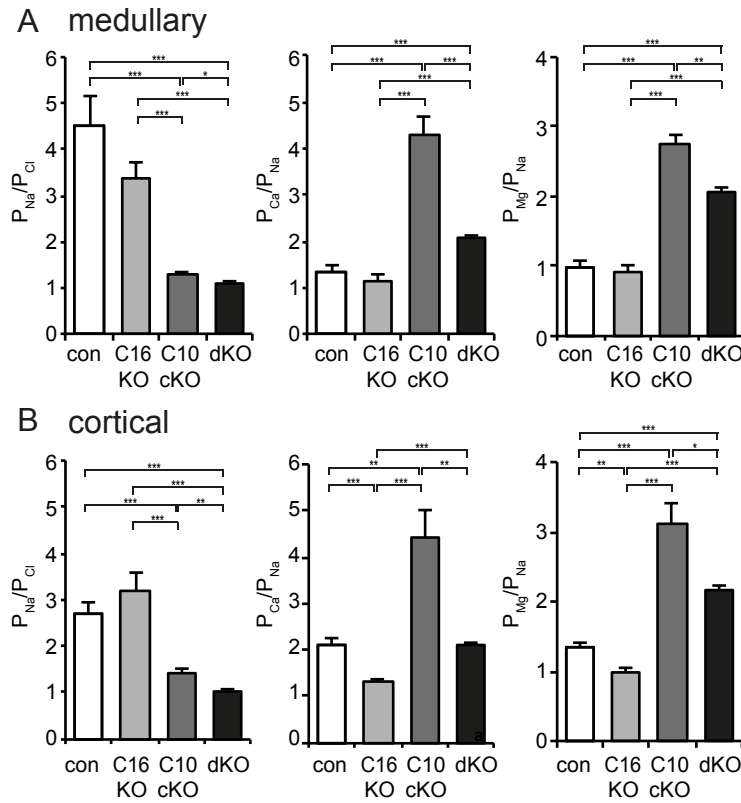


Figure 5 Tubular permeability ratios of isolated perfused mTAL and cTAL

Relative ion permeability P_{Na}/P_{Cl} calculated from NaCl dilution voltages and relative ion permeabilities P_{Mg}/P_{Na} and P_{Ca}/P_{Na} calculated from bi-ionic diffusion voltages from mTAL (A) and cTAL (B). (A) In mTAL, absence of claudin-10 reduces cation selectivity and increases P_{Mg}/P_{Na} and P_{Ca}/P_{Na} . Additional claudin-16 deficiency in dKO reverses this effect at least partially. (B) Absence of claudin-10 reduces cation selectivity. Deficiency for claudin-16 decreases and for claudin-10 increases P_{Ca}/P_{Na} and P_{Mg}/P_{Na} . In dKO P_{Ca}/P_{Na} is normalized and P_{Mg}/P_{Na} increased less in comparison to C10 cKO. Data are shown as mean \pm SEM. $n=7-19$. * $p<0.05$, ** $p<0.01$, *** $p<0.001$ in one-way ANOVA with Holm-Bonferroni post-hoc test.

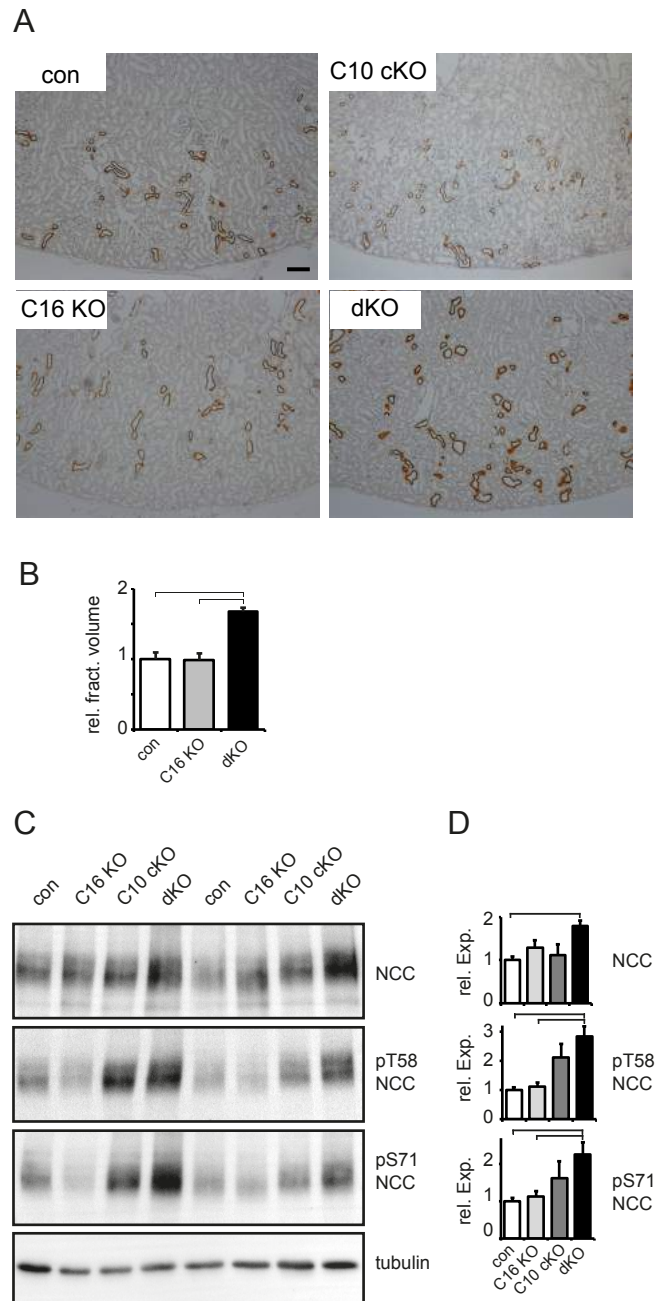


Figure 6 Expression and activity of NCC

(A) Immunohistochemical analysis of NCC Expression in cortical kidney sections of con, C16 KO, C10 cKO and dKO. Scale bar 200 μ m (B) Quantification of the fractional volume of DCT segments of C16 KOs and dKOs normalized to control. Brackets indicate $p < 0.001$, in one-way ANOVA with Holm-Bonferroni post-hoc test. (C) Western Blot analysis of kidney lysates of con, C16 KO, C10 cKO and dKO mice using antisera detecting NCC and phosphorylated NCC (pT58: phosphorylated Threonine 58, pS71: phosphorylated Serine 71). (D) Densitometric analysis of western blot analysis. Bar graphs represent mean of signal intensity ratios relative to tubulin normalized to mean of controls \pm SEM (n= 4). Brackets indicate $p < 0.05$, in one-way ANOVA with Holm-Bonferroni post-hoc test.

	Gene	control	C16 KO	<i>P</i> C16 vs. con	C10 cKO	<i>P</i> C10 vs. con	<i>P</i> C10 vs. C16	dKO	<i>P</i> dKO vs. con	<i>P</i> dKO vs. C16 KO	<i>P</i> dKO vs. C10 cKO
claudin-11	Cldn11	1.00 ± 0.05	1.09 ± 0.07		0.35 ± 0.01	***	***	0.32 ± 0.01	***	***	
claudin-14	Cldn14	1.00 ± 0.07	0.94 ± 0.15		1.20 ± 0.12			0.96 ± 0.09			
claudin-19	Cldn 19	1.00 ± 0.02	0.91 ± 0.06		1.12 ± 0.11			1.26 ± 0.06	*	*	
TRPV5	Trpv5	1.00 ± 0.05	0.99 ± 0.07		1.00 ± 0.01			1.05 ± 0.07			
NCX1	Slc8a1	1.00 ± 0.05	1.62 ± 0.13	*	0.43 ± 0.05	*	*	1.50 ± 0.10	*		*
CaSR	Casr	1.00 ± 0.13	0.87 ± 0.06		1.03 ± 0.10			1.15 ± 0.14			
TRPM6	Trpm6	1.00 ± 0.07	1.27 ± 0.07	*	0.48 ± 0.01	**	***	1.62 ± 0.08	**	*	***
Parvalbumin	Pvalb	1.00 ± 0.04	1.17 ± 0.28		0.07 ± 0.00	***	*	1.92 ± 0.24	*		**
CNNM2	Cnnm2	1.00 ± 0.04	1.22 ± 0.12		0.82 ± 0.07			1.28 ± 0.05	*		*
SLC41a3	Slc41a3	1.00 ± 0.08	0.95 ± 0.15		0.82 ± 0.05	*		1.12 ± 0.13			*
NCC	Slc12a3	1.00 ± 0.03	1.29 ± 0.06	*	0.66 ± 0.05	**	**	1.54 ± 0.07	**	*	*
NKCC2	Slc12a1	1.00 ± 0.17	1.02 ± 0.19		1.03 ± 0.07			1.10 ± 0.21			
		n = 4	n = 4		n = 4			n = 4			

Table 2 Gene array analysis of genes involved in distal tubular electrolyte transport

Selected gene expression data from total kidneys of claudin KO mouse models described in this study. Expression values are given relative to control mice. Data are shown as mean ± SEM. * p<0.05, ** p<0.01, *** p<0.001 in one-way ANOVA with Holm-Bonferroni post-hoc test

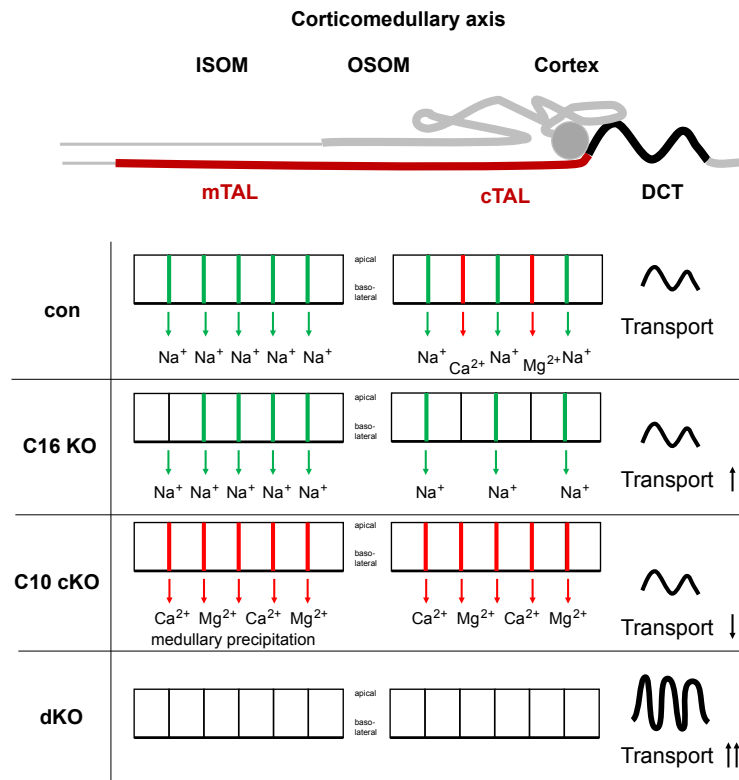
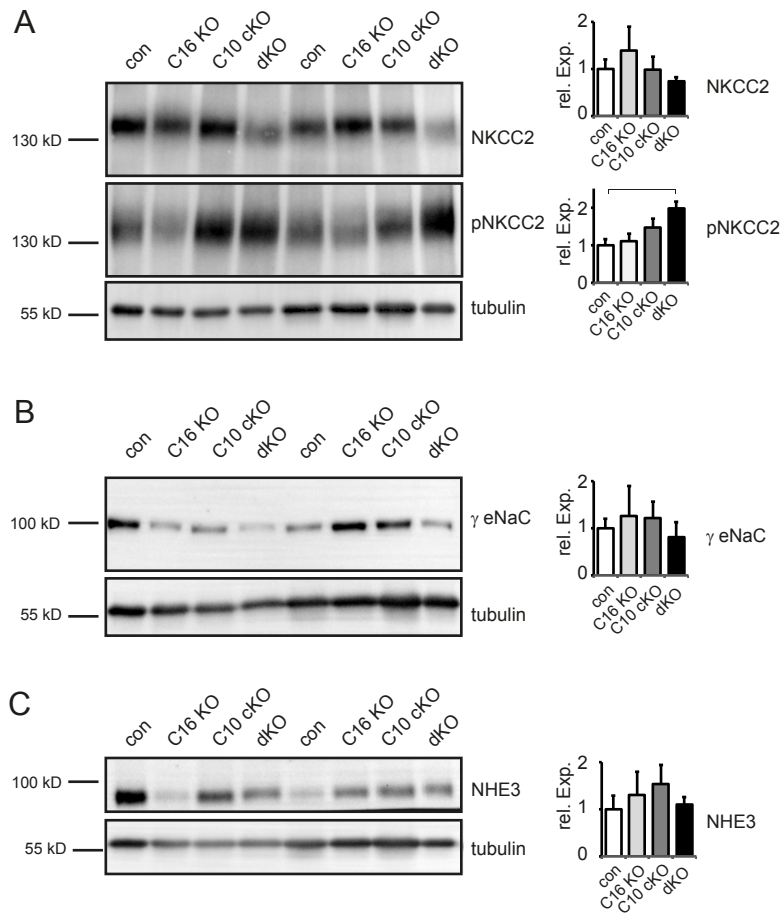


Figure 7 Paracellular TAL transport and effects on DCT transport

Simplified TAL epithelial model with claudin-10 positive (green) and claudin-16 positive (red) tight junctions together with the preferred cation. DCT pictogram to symbolize increase in fractional volume.



Supplemental Figure Expression of renal sodium transport proteins

Western Blot analysis of kidney lysates of con, C16 KO, C10 cKO and dKO mice using antisera detecting NKCC2, phosphorylated NKCC2 (A), eNaC γ -subunit (B) and NHE3 (C) Densitometric analysis of western blot analysis. Bar graphs represent mean of signal intensity ratios relative to tubulin normalized to mean of controls \pm SEM (n= 4). Brackets indicate $p < 0.05$, in one-way ANOVA with Holm-Bonferroni post-hoc test.